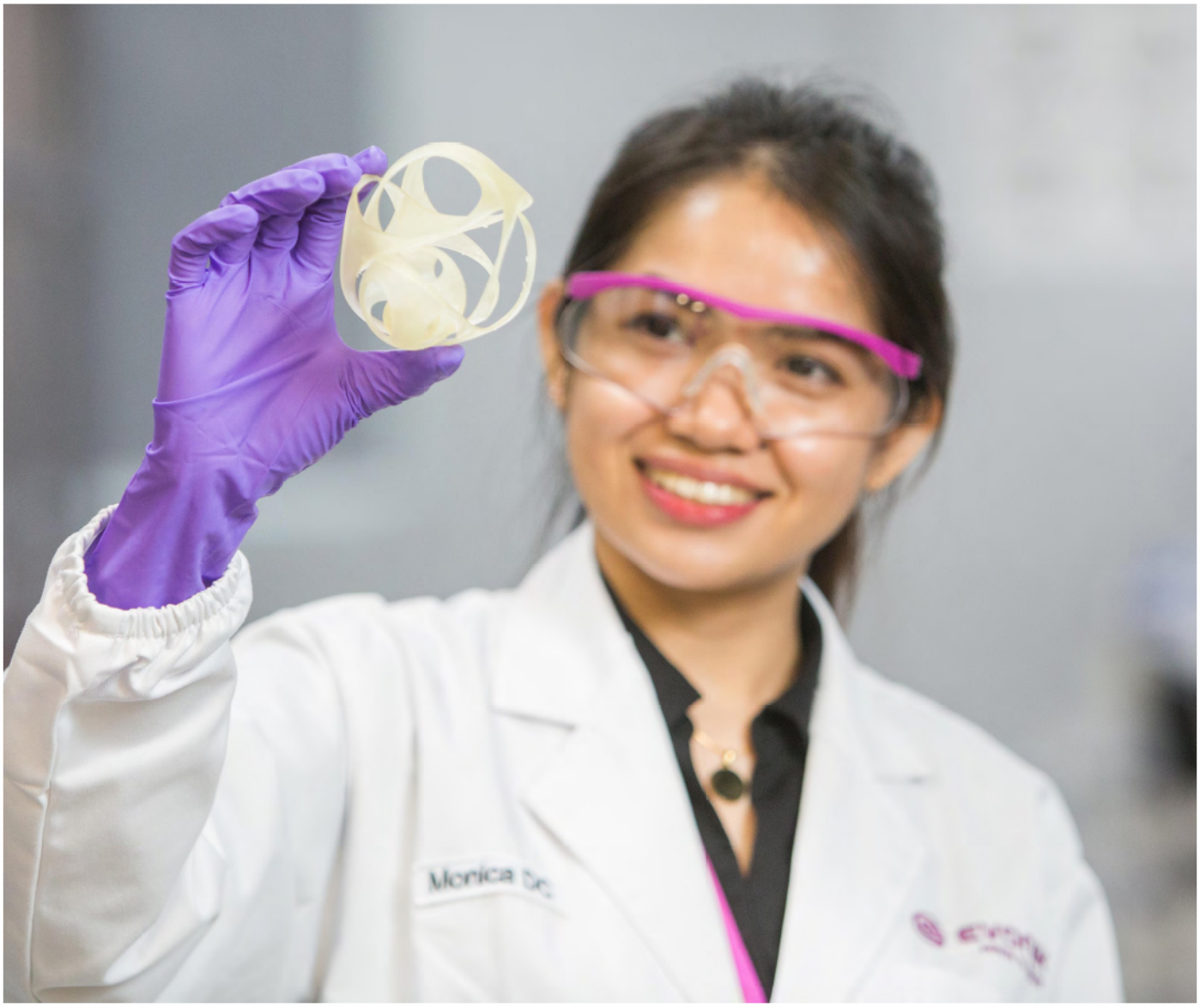

# Pushing the boundaries of chemistry? It takes #HumanChemistry

Make your curiosity and talent as a chemist matter to the world with a specialty chemicals leader. Together, we combine cutting-edge science with engineering expertise to create solutions that answer real-world problems. Find out how our approach to technology creates more opportunities for growth, and see what chemistry can do for you at:

**evonik.com/career**

EVONIK
Leading Beyond Chemistry

ADVANCED FUNCTIONAL MATERIALS
www.afm-journal.de

# F and N Rich Solid Electrolyte for Stable All-Solid-State Battery

*Hongli Wan, Jiaxun Zhang, Jiale Xia, Xiao Ji, Xinzi He, Sufu Liu, and Chunsheng Wang**

**The instability of sulfide solid electrolytes to Li anode and high-voltage $LiNi_{0.8}Mn_{0.1}Co_{0.1}O_2$ (NMC811) cathodes limits the cyclic performance of all-solid-state lithium battery (ASSLB). Herein, the stability of $Li_6PS_5Cl$ against Li anode is enhanced by mixing a small amount (0.32 wt%) of $CuF_2$-$LiNO_3$ (CL) into $Li_6PS_5Cl$ electrolyte layer to in-situ form a mixed-conductive-lithiophobic and self-healing LiF-$Li_3N$-Cu solid electrolyte interphase (SEI) at $Li_6PS_5Cl$-CL/Li interface. The critical current density (CCD) of $Li_6PS_5Cl$-$CuF_2$-$LiNO_3$ increases to 1.4 mA cm$^{-2}$/1.4 mAh cm$^{-2}$ at room temperature, which is much higher than that of pristine $Li_6PS_5Cl$ (0.4 mA cm$^{-2}$/0.4 mAh cm$^{-2}$) even though mixing 0.32 wt% CL into $Li_6PS_5Cl$ slightly reduces the ionic conductivity from $2.9 \times 10^{-3}$ to $1.5 \times 10^{-3}$ S cm$^{-1}$. The compatibility of $Li_6PS_5Cl$-CL electrolyte to single-crystalline NMC811 (S-NMC811) is further enhanced by adding a small amount (0.02 wt%) of $AlF_3$ into $Li_6PS_5Cl$-CL forming $Li_6PS_5Cl$-$CuF_2$-$LiNO_3$-$AlF_3$ ($Li_6PS_5Cl$-CLA) as a cathode electrolyte and by doing $Cl^-$ on S-NMC811 (Cl@S-NMC811) surface. The Cl@S-NMC811-$Li_6PS_5Cl$-CLA|$Li_6PS_5Cl$-CL|Li cells with areal capacity of 2.55 mAh cm$^{-2}$ achieve a capacity retention of 69.4% after 100 cycles at 1C (1C = 200 mAh g$^{-1}$). Adding a small amount of SEI and cathode/electrolyte interphase (CEI) former into the sulfide electrolytes with minimal reduction (48.3%) of ionic conductivity is an effective method to enhance the performance of ASSLB.**

## 1. Introduction

All-solid-state battery employing a high-voltage and high-capacity Ni-rich layered oxide $LiNi_xMn_yCo_{1-x-y}O_2$ ($x$>0.6, NMC) cathode, metallic lithium anode, and high ionic conductivity sulfide solid electrolyte (SSE) (NMC|SSE|Li cell) is promising to reach high cell-level energy density of 400 Wh kg$^{-1}$.[1] Among them, $LiNi_{0.8}Mn_{0.1}Co_{0.1}O_2$ (NMC811) shows high reversible capacity of around 200 mAh g$^{-1}$ and $Li_6PS_5Cl$ sulfide electrolyte has a high ionic conductivity of >$10^{-3}$ S cm$^{-1}$. However, the NMC811|SSE|Li cells still suffer from a fast capacity decay because sulfide solid electrolyte is not stable to both Li anode and NMC811 cathode.[2–7] $Li_6PS_5Cl$ electrolyte will react with NMC811 at a high potential forming a highly resistive cathode/electrolyte interphase (CEI). Moreover, side reaction on NMC811 surface also promotes the structure degradation and cracks evolution of NMC811, which reduces the Coulombic efficiency (CE) and cycle life.[8] To minimize the side reaction, single-crystalline NMC811 (S-NMC811) particles with a higher structure stability than poly-crystalline NMC811 (P-NMC811) have been used in all-solid-state Li batteries and showed improved cycling stability.[1,5] The structure stability of S-NMC811 can be further enhanced by halogen doping.[9–11] Specifically, doping F into $Li_6PS_5Cl$ electrolyte can improve the oxidation stability of $Li_6PS_5Cl$ electrolyte. However, F doping also significantly reduces the ionic conductivity[12] due to the high bonding between F and Li, which will reduce the rate capability of ASSLB. Mixing of highly oxidation-resistive compounds into $Li_6PS_5Cl$ electrolyte should also enhance the oxidation stability of $Li_6PS_5Cl$ electrolytes.

In addition to the compatibility of $Li_6PS_5Cl$ electrolyte to NMC811 cathode, the lithium dendrite growth into $Li_6PS_5Cl$ electrolyte on Li anode side is even more challenged because the SEI formed from reduction of $Li_6PS_5Cl$ cannot block the Li dendrite.[13,14] LiF has a high interface energy against Li, which can effectively suppress Li dendrite growth.[15–17] However, the ultra-low ionic conductivity of LiF also increases cell overpotential. We have demonstrated that mixing a high ionic conductivity $Li_3N$ into LiF can reduce cell overpotential, while still maintain the high lithium dendrite suppression capability.[15] Li plating overpotential and Li dendrite can be further suppressed by adding lithiophobic and electronic conductive component (such as Cu and Ni) into the ionic conductive and lithiophobic $Li_3N$-LiF interlayer forming a mixed conductive lithiophobic interlayer, where the lithiophobic component will suppress the Li dendrite and electronic conducting Cu can reduce the Li plating overpotential. Such a mixed conductive lithiophobic interlayer has not been reported yet. Moreover, all reported efforts focus on inserting an artificial lithiophobic, lithiophilic, or lithiophobic–lithiophilic interlayer between Li and solid-state electrolyte to suppress lithium dendrite growth.[18–21] However, the interlayer will break during charge/discharge process due to the large volume change, and lithium can penetrate through the passivation layer and grow inside the $Li_6PS_5Cl$ electrolyte. Therefore, all reported electrode/SSE interface modification is lack of self-healing capability and can only stabilize the solid-state Li batteries during initial charge/discharge cycles, and fails once passivation layer breaks.

H. L. Wan, J. X. Zhang, J. L. Xia, X. Ji, X. Z. He, S. F. Liu, C. S. Wang
Department of Chemical and Biomolecular Engineering
University of Maryland
College Park, MD 20740, USA
E-mail: cswang@umd.edu

The ORCID identification number(s) for the author(s) of this article can be found under https://doi.org/10.1002/adfm.202110876.

DOI: 10.1002/adfm.202110876

 

Herein, such a mixed ionic/electronic conductive and lithiophobic interlayer (LiF-$Li_3N$-Cu) was in-situ formed at $Li_6PS_5Cl$/Li interface by adding 0.32 wt% of $CuF_2$-$LiNO_3$ (CL) into $Li_6PS_5Cl$ electrolyte layer. During Li plating/stripping cycles, the SEI former ($CuF_2$-$LiNO_3$) on the surface of $Li_6PS_5Cl$ will be reduced into LiF-$Li_3N$-Cu. Even though the LiF-$Li_3N$-Cu layer at $Li_6PS_5Cl$/Li interface was broken and the lithium dendrite grown into the $Li_6PS_5Cl$, it will be consumed by the surface SEI former, and the newly formed interlayer will also be capable to suppress lithium dendrite. The self-healing property of the interlayer can only be achieved by surface modification of entire electrolyte. The $CuF_2$-$LiNO_3$ modification of bulk electrolyte significantly improved critical current density (CCD) from 0.4 mA $cm^{-2}$/0.4 mAh $cm^{-2}$ for pristine $Li_6PS_5Cl$ to 1.4 mA $cm^{-2}$/1.4 mAh $cm^{-2}$ for $Li_6PS_5Cl$-$CuF_2$-$LiNO_3$ at room temperature. To suppress the side reaction and crack evolution of S-NMC811 cathodes, 0.34 wt% of $CuF_2$-$LiNO_3$-$AlF_3$ (CLA) CEI former was added into $Li_6PS_5Cl$ electrolyte and $Cl^-$ was doped onto S-NMC811 surface in the S-NMC811 cathode since $AlF_3$ can improve the structure stability of S-NMC811.[22,23] The Cl@S-NMC811-$Li_6PS_5Cl$-$CuF_2$-$LiNO_3$-$AlF_3$|$Li_6PS_5Cl$-$CuF_2$-$LiNO_3$|Li (Cl@S-NMC811-$Li_6PS_5Cl$-CLA|$Li_6PS_5Cl$-CL|Li) cell with an areal capacity of 2.55 mAh $cm^{-2}$ achieved a capacity retention of 69.4% after 100 cycles at 1C (1C = 200 mAh $g^{-1}$). It is the first report for sulfide solid electrolyte that can be stable for both metallic lithium anode and high-voltage NMC811 cathode through a simple compound mixing procedure.

## 2. Results and Discussion

$Li_6PS_5Cl$-$CuF_2$-$LiNO_3$ ($Li_6PS_5Cl$-CL) electrolyte was obtained by homogenously mixing $CuF_2$-$LiNO_3$-DME solution with $Li_6PS_5Cl$ followed by vacuum dried at 80 °C to remove DME solvent (detailed preparation method can be found in Supporting Information). $LiNO_3$ was used as an agent to dissolve $CuF_2$ in DME solvent and to form highly ionic conductive $Li_3N$ after reduction. As shown in Figure S1 (Supporting Information), after $Li_6PS_5Cl$ electrolyte was mixed with $CuF_2$-$LiNO_3$-DME solvent and dry, the main phase of $Li_6PS_5Cl$ remains unchanged, implying that nano-sized $CuF_2$-$LiNO_3$ was only coated on $Li_6PS_5Cl$ particle surface, which improves the stability of $Li_6PS_5Cl$ to Li metal by forming a lithiophobic LiF-$Li_3N$-Cu interphase during Li plating/stripping cycles. Adding only 0.32 wt% of $CuF_2$-$LiNO_3$ into $Li_6PS_5Cl$ electrolyte significantly increased CCD from 0.4 mA $cm^{-2}$/0.4 mAh $cm^{-2}$ to 1.4 mA $cm^{-2}$/1.4 mAh $cm^{-2}$ (**Figure 1**a). Besides, the Li plating/stripping overpotential in Li|$Li_6PS_5Cl$-CL|Li cell is smaller than that in Li|$Li_6PS_5Cl$|Li cell (Figure 1a before short circuit) even the ionic conductivity of electrolyte decreased from $2.9 \times 10^{-3}$ to $1.5 \times 10^{-3}$ S $cm^{-1}$ by adding of $CuF_2$-$LiNO_3$ (Figure S2, Supporting Information), implying the LiF-$Li_3N$-Cu interlayer has a low interfacial resistance than the interlayer formed from reduction of $Li_6PS_5Cl$. The weight ratio of $CuF_2$ and $LiNO_3$ also affects the CCD of $Li_6PS_5Cl$-$CuF_2$-$LiNO_3$ composite electrolyte. As shown in Figure S3 (Supporting Information), the CCD of $Li_6PS_5Cl$-$CuF_2$-$LiNO_3$ electrolytes increased from 0.8 mA $cm^{-2}$/0.8 mAh $cm^{-2}$ (Figure S3a, Supporting Information) to 1.0 mA $cm^{-2}$/1.0 mAh $cm^{-2}$ (Figure S3b, Supporting Information) when the $CuF_2$/$LiNO_3$ weight ratio decreased from 20/40 to 20/50. The uniform distribution of $CuF_2$-$LiNO_3$ around the surface of $Li_6PS_5Cl$ electrolyte also affects the performance of $Li_6PS_5Cl$-CL electrolyte. As shown in Figure S4 (Supporting Information), even though the much higher ionic conductivity of hand-mixed $Li_6PS_5Cl$-CL ($2.9 \times 10^{-3}$ S $cm^{-1}$, mixing $Li_6PS_5Cl$ powder with $CuF_2$ and $LiNO_3$ powder) compared with the wet-mixed $Li_6PS_5Cl$-CL (mixing $Li_6PS_5Cl$ with $CuF_2$-$LiNO_3$-DME solvent and followed by heat treatment at 80 °C), the CCD of hand-mixed $Li_6PS_5Cl$-CL was only 0.5 mA $cm^{-2}$/0.5 mAh $cm^{-2}$ (Figure S5, Supporting Information).

The $CuF_2$ and $LiNO_3$ at the interface of $Li_6PS_5Cl$-CL/Li will be reduced by Li forming lithiophobic LiF-$Li_3N$-Cu interlayer. Lithiophobic LiF has a high interface energy, which can suppress Li dendrite, while $Li_3N$-Cu with a balanced ionic and electronic conductivity can decrease Li plating overpotential. The formation of LiF-$Li_3N$-Cu interlayer was confirmed by cross-section scanning electron microscope (SEM), energy dispersive spectroscopy (EDS), and time-of-flight secondary ion mass spectroscope (ToF-SIMS). Figure 1b,c shows the cross-section SEM and backscattering electron images of $Li_6PS_5Cl$-CL/Li interface after depositing 0.5 mAh $cm^{-2}$ of Li between $Li_6PS_5Cl$-CL and SS (SS = stainless steel). A Li layer above the electrolyte layer was clearly observed. No lithium dendrites inside the $Li_6PS_5Cl$-CL composite electrolyte were observed after Li plating. Besides, elemental distribution images along the depth of the sputtered crater at $Li_6PS_5Cl$-CL composite electrolyte reveal that F and N were rich at the interface of $Li_6PS_5Cl$-CL/Li after Li plating/stripping cycles (Figure 1d,e) because $CuF_2$-$LiNO_3$ was enriched on $Li_6PS_5Cl$-CL membrane surface after compression of $Li_6PS_5Cl$-CL powders in the membrane formation process (Figures S6 and S7, Supporting Information). The formation of LiF-$Li_3N$-Cu interlayer after Li plating/stripping cycles further enhanced the F and N surface enrichment on $Li_6PS_5Cl$-CL (Figure S8, Supporting Information). Such an interlayer enables the Li|$Li_6PS_5Cl$-CL|Li symmetric cell to be stably charged/discharged at 0.2 mA $cm^{-2}$/0.2 mAh $cm^{-2}$ and 0.5 mA $cm^{-2}$/0.5 mAh $cm^{-2}$ for 120 cycles (Figure 1f). Apart from the enhanced lithium dendrite suppressing capability, the particle size of $Li_6PS_5Cl$-CL electrolyte was also reduced after $CuF_2$-$LiNO_3$-DME treatment (Figure S9b, Supporting Information) compared with the pristine $Li_6PS_5Cl$ electrolyte (Figure S9a, Supporting Information), which increases the triple-phase contacts in S-NMC811 cathode, thus accelerating the reaction kinetics.

Single-crystalline NMC cathodes have been reported to have a long cycle life than poly-crystalline NMC in liquid organic electrolytes.[1] S-NMC811 and P-NMC811 cathodes were evaluated in all-solid-state battery using $Li_6PS_5Cl$ electrolytes. Since NMC811 is not stable in $Li_6PS_5Cl$ electrolytes and normally $LiNbO_3$ has to be coated on NMC811 surface to prevent the surface reaction with $Li_6PS_5Cl$ electrolytes. Therefore, $LiNbO_3$ coated S-NMC811 ($LiNbO_3$@S-NMC811) and P-NMC811 ($LiNbO_3$@P-NMC811) particles were used as the cathode active materials. Figure S10 (Supporting Information) compared the electrochemical performance of $LiNbO_3$@S-NMC811 cathodes to that of $LiNbO_3$@P-NMC811 cathodes using $LiNbO_3$@NMC811-$Li_6PS_5Cl$|$Li_6PS_5Cl$-CL|Li cells, where $Li_6PS_5Cl$ was used as electrolyte in NMC811 cathode layer, $Li_6PS_5Cl$-CL electrolyte was used in electrolyte layer. $LiNbO_3$@S-NMC811 cathodes show a much higher capacity and more stable cyclic performance than that of

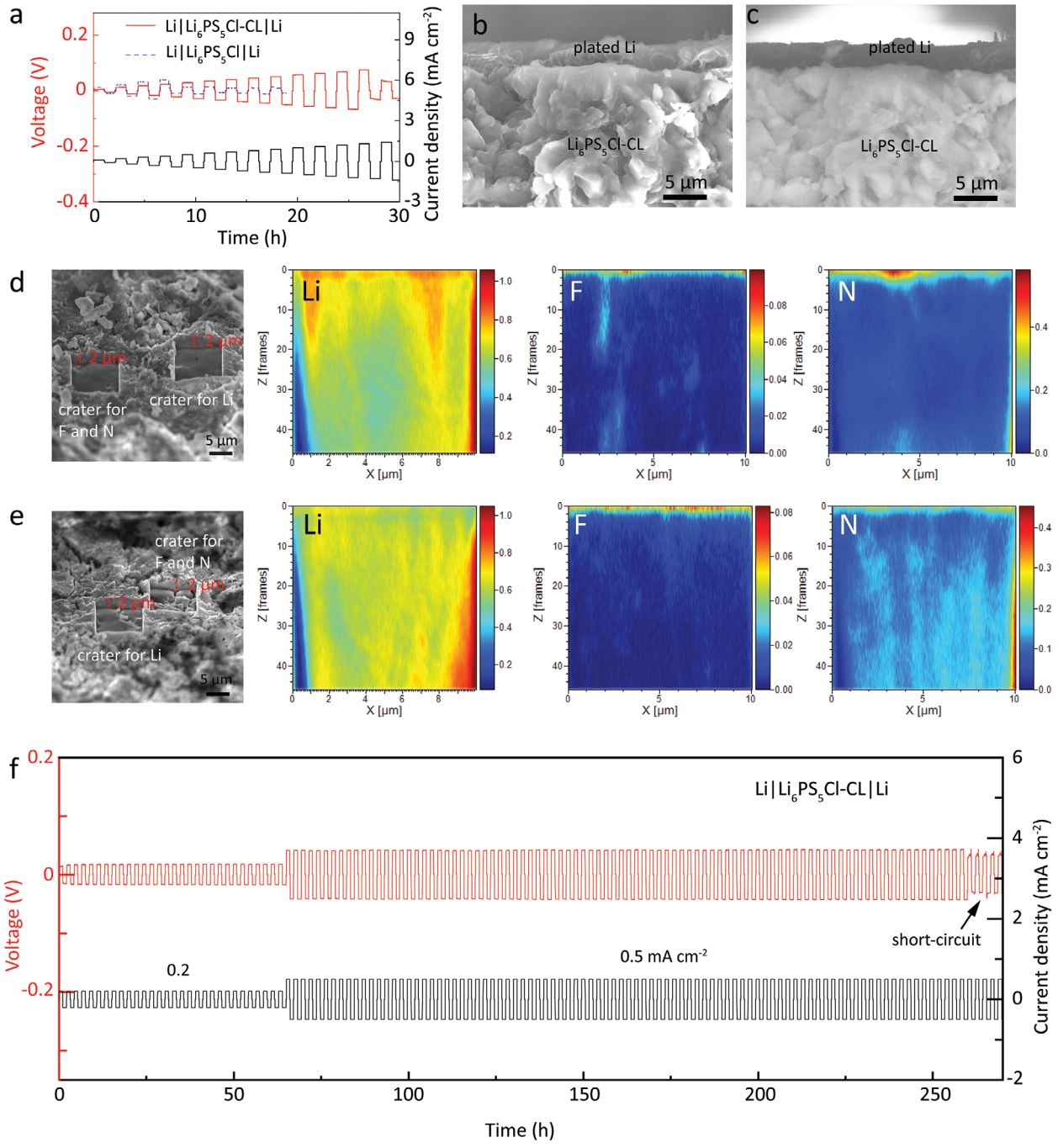


**Figure 1.** a) Voltage profile of Li|$Li_6PS_5Cl$|Li cell at step-increased current densities using the $Li_6PS_5Cl$ with and without mixing of $CuF_2$-$LiNO_3$ (CL). b) Cross-section scanning electron microscope (SEM) and c) back-scattering electron image of $Li_6PS_5Cl$-CL/Li (deposited) interface after Li plating at the interface of $Li_6PS_5Cl$-CL/SS (SS = stainless steel). Li, N, and F distribution along the depth of the sputtered crater at $Li_6PS_5Cl$-CL surface after d) Li plating and e) Li stripping (1 frame = 46.5 nm). f) Voltage profile of Li|$Li_6PS_5Cl$-CL|Li cell at 0.2 mA $cm^{-2}$/0.2 mAh $cm^{-2}$ and 0.5 mA $cm^{-2}$/0.5 mAh $cm^{-2}$.

$LiNbO_3$@P-NMC811 cathodes at 1C (1C = 200 mAh $g^{-1}$) and temperature of 80 °C. The enhanced electrochemical performance of $LiNbO_3$@S-NMC811 cathodes is attributed to the more stable structure and the smaller particle size of S-NMC811 (Figure S11b, Supporting Information) than that of P-NMC811 (Figure S11a, Supporting Information). Therefore, S-NMC811 was selected as cathode material for electrochemical performance evaluation.

It has been reported that the fluoride CEI can enhance the structure stability of NMC811 cathode in organic liquid electrolyte due to the high oxidation stability of fluoride CEI.[22,24–26] To suppress side reaction between $Li_6PS_5Cl$ and $LiNbO_3$@S-NMC811, we added 0.02 wt% of $AlF_3$ into $Li_6PS_5Cl$-CLA as cathode electrolyte but still used $Li_6PS_5Cl$-CL in electrolyte layer. As shown in Figure S12 (Supporting Information), the

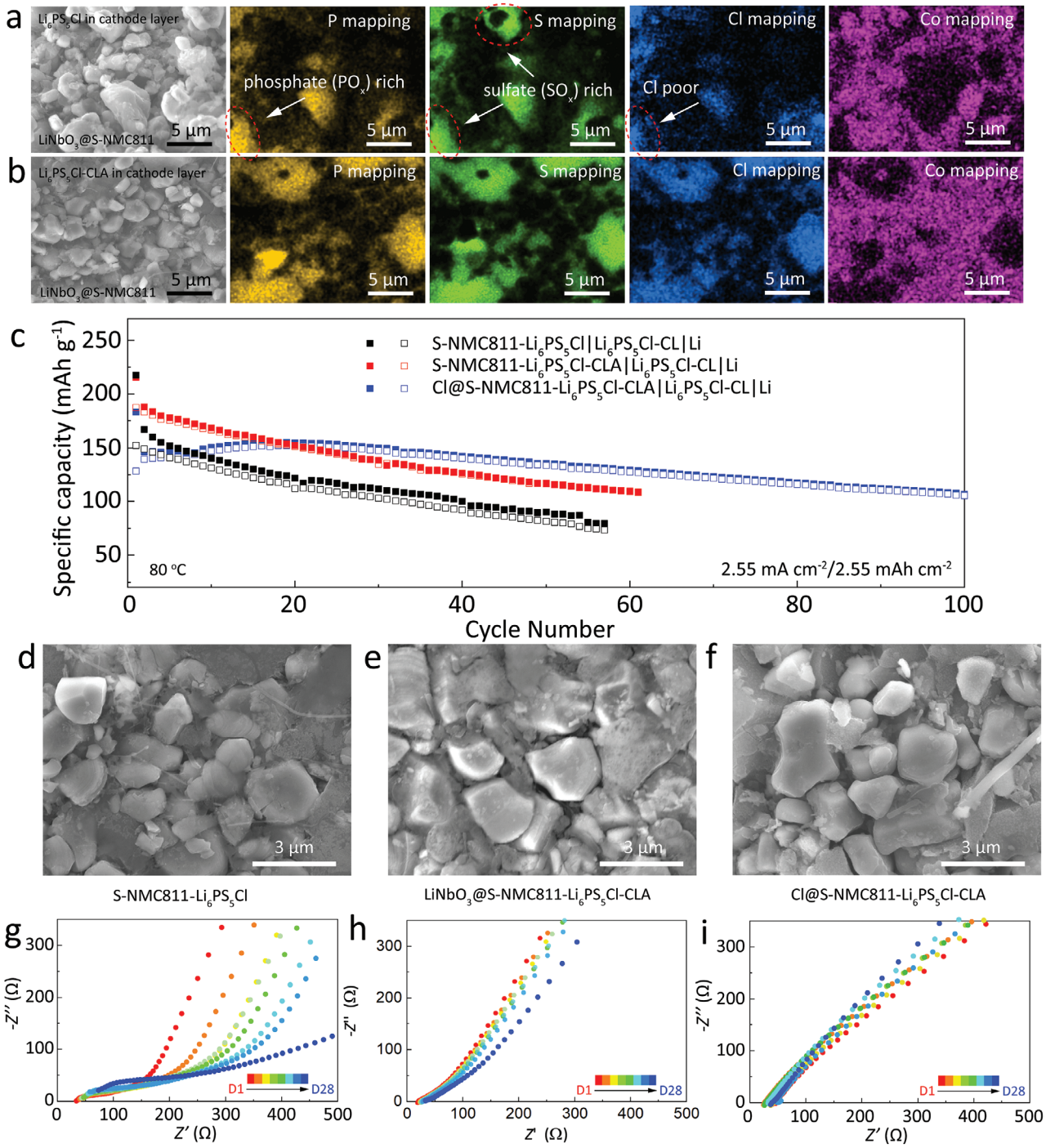


**Figure 2.** Scanning electron microscope (SEM) and energy dispersive spectroscopy (EDS) mapping of cycled a) $LiNbO_3$@S-NMC811-$Li_6PS_5Cl$ and b) $LiNbO_3$@S-NMC811-$Li_6PS_5Cl$-CLA cathode. c) Cyclic performance of S-NMC811-$Li_6PS_5Cl$|$Li_6PS_5Cl$-CL|Li, S-NMC811-$Li_6PS_5Cl$-CLA|$Li_6PS_5Cl$-CL|Li and Cl@S-NMC811-$Li_6PS_5Cl$-CLA|$Li_6PS_5Cl$-CL|Li cell, all the cells were tested at 2.55 mA $cm^{-2}$/2.55 mAh $cm^{-2}$ and temperature of 80 °C. SEM images of d) S-NMC811-$Li_6PS_5Cl$, e) $LiNbO_3$@S-NMC811-$Li_6PS_5Cl$-CLA, and f) Cl@S-NMC811-$Li_6PS_5Cl$-CLA cathode after cycling. Impedance evolution of g) S-NMC811-$Li_6PS_5Cl$|$Li_6PS_5Cl$-CL|Li, h) $LiNbO_3$@S-NMC811-$Li_6PS_5Cl$-CLA|$Li_6PS_5Cl$-CL|Li, and i) Cl@S-NMC811-$Li_6PS_5Cl$-CLA|$Li_6PS_5Cl$-CL|Li all-solid-state lithium battery during open-circuit for 28 days.

cycling stability of $LiNbO_3$@S-NMC811 using $Li_6PS_5Cl$-CLA as cathode electrolyte is much better than that using $Li_6PS_5Cl$-CL as cathode electrolyte at 2.55 mA $cm^{-2}$/2.55 mAh $cm^{-2}$ due to the reduced side reactions between $LiNbO_3$@S-NMC811 and $Li_6PS_5Cl$-CLA electrolyte in cathode. The higher compatibility of $LiNbO_3$@S-NMC811 and $Li_6PS_5Cl$-CLA electrolyte at high potential was evidenced by the uniform distribution of elemental P, S, and Cl around $LiNbO_3$@S-NMC811 particles

(**Figure 2**b). However, for $LiNbO_3$@S-NMC811-$Li_6PS_5Cl$ composite cathode, P-rich, S-rich but Cl-poor regions (as marked in Figure 2a) at interface of $LiNbO_3$@S-NMC811/$Li_6PS_5Cl$ can be clearly observed in $Li_6PS_5Cl$ electrolyte (without adding CLA additive), implying the formation of sulfate and phosphate species due to the interfacial reactions. Therefore, $Li_6PS_5Cl$-CLA was selected as cathode electrolyte.

Although $LiNbO_3$@S-NMC811-$Li_6PS_5Cl$-CLA|$Li_6PS_5Cl$-CL|Li cell shows good cycling stability, coating $LiNbO_3$ on S-NMC811 is time consuming and requires a high temperature annealing process under oxygen. Herein, we developed a $Cl^-$ doped S-NMC811 (Cl@S-NMC811) cathode (Figure S13, Supporting Information) to ameliorate the side reactions between S-NMC811 and $Li_6PS_5Cl$-CLA electrolyte in cathode layer. We compared the electrochemical performance of Cl@S-NMC811 with that of pristine S-NMC811 by using $Li_6PS_5Cl$-CLA (or $Li_6PS_5Cl$) electrolyte in cathode layer, and $Li_6PS_5Cl$-CL in electrolyte layer. As shown in Figure 2c, the capacity retention of Cl@S-NMC811-$Li_6PS_5Cl$-CLA|$Li_6PS_5Cl$-CL|Li (blue square) cell was 69.4% (calculated based on the highest reversible capacity), which is much higher than that of pristine S-NMC811 in $Li_6PS_5Cl$-CLA (red square) and $Li_6PS_5Cl$ (black square) cathode electrolyte. The cyclic performance of Cl@S-NMC811 cathodes is comparable to that of $LiNbO_3$@S-NMC811 cathode with capacity retention of 68.8% after 100 cycles at 2.55 mA $cm^{-2}$/2.55 mAh $cm^{-2}$ (Figure S12, Supporting Information). The reduced side reactions between S-NMC811 and electrolyte by using $Cl^-$ doped S-NMC811 and $Li_6PS_5Cl$-CLA electrolyte in cathode layer also suppress the cracking initiated from surface stress/strain.[3] As shown in Figure 2e,f, the crack evolution of S-NMC811 was obviously ameliorated in Cl@S-NMC811-$Li_6PS_5Cl$-CLA (Figure 2f and Figure S14, Supporting Information) and $LiNbO_3$@S-NMC811-$Li_6PS_5Cl$-CLA cathode compared with the pristine S-NMC811-$Li_6PS_5Cl$ cathode (Figure 2d). The good compatibility of Cl@S-NMC811 to $Li_6PS_5Cl$-CLA can also be evidenced by the more stable EIS spectra of Cl@S-NMC811-$Li_6PS_5Cl$-CLA|$Li_6PS_5Cl$-CL|Li cell (Figure 2i) than that of $LiNbO_3$@S-NMC811-$Li_6PS_5Cl$-CLA|$Li_6PS_5Cl$-CL|Li cell (Figure 2h) during storage at open circuit for 28 days. In sharp contrast, the impedance of S-NMC811-$Li_6PS_5Cl$|$Li_6PS_5Cl$-CL|Li cell increases rapidly during 28 days in open-circuit (Figure 2g).

The stability of Li to $Li_6PS_5Cl$ and $Li_6PS_5Cl$-CL electrolytes, and the stability of $Li_6PS_5Cl$-CLA electrolyte to Cl@S-NMC811 and S-NMC811 cathodes were monitored by using a three-electrode cell with a Li reference electrode (the cell structure was shown in Figure S15, Supporting Information). As shown in **Figure 3**a and Figure S16 (Supporting Information), Li anode potential (versus Li RE) during Li plating and followed resting in $Li_6PS_5Cl$-CL electrolyte are almost constant due to formation of a stable interlayer between $Li_6PS_5Cl$-CL electrolyte and Li anode. However, the overpotential of Li anode using $Li_6PS_5Cl$ electrolyte was larger than that using $Li_6PS_5Cl$-CL electrolyte, due to the serious side reactions between $Li_6PS_5Cl$ and Li anode during Li plating process (Figure S16, Supporting Information). As for S-NMC811 cathode, the Cl-doping on S-NMC811 increased the cathode overpotential (the potential drop after resting in Figure 3a), which slightly reduced the charge capacity (Figure 3a,b). However, Cl@S-NMC811 cathode has a much slower potential decay (Figure 3a) than S-NMC811 (Figure 3b) during resting due to the formation of the passivated interlayer between Cl@S-NMC811 and $Li_6PS_5Cl$-CLA. However, such a passivated layer also leads to slightly reduced reversible capacity of Cl@S-NMC811 cathode in the first few cycles (Figure 2c) due to the slightly high overpotential (Figure 3a). However, the reversible capacity of Cl@S-NMC811 was much more stable than that of S-NMC811 (Figure 2c) due to enhanced structure

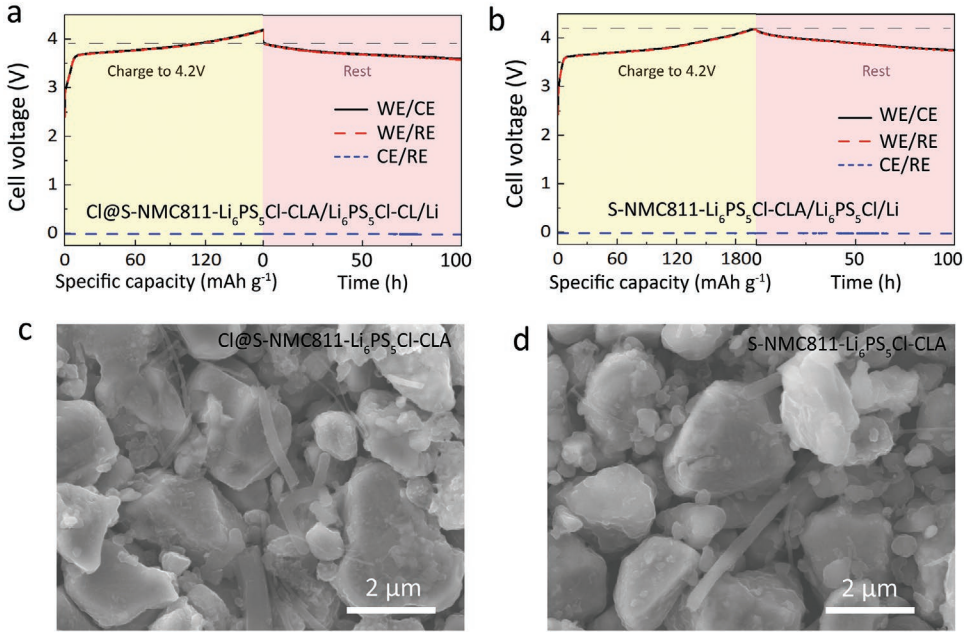


**Figure 3.** Voltage profile of a) Cl@S-NMC811-$Li_6PS_5Cl$-CLA|$Li_6PS_5Cl$-CL|Li and b) S-NMC811-$Li_6PS_5Cl$-CLA|$Li_6PS_5Cl$|Li three-electrode cell. Scanning electron microscope (SEM) images of c) Cl@S-NMC811-$Li_6PS_5Cl$-CLA and d) S-NMC811-$Li_6PS_5Cl$-CLA cathode after resting.

stability of Cl@S-NMC811 cathode, as evidenced by the absence of cracks in Cl@S-NMC811 composite cathode at the end of resting (Figure 3c). In sharp contrast, obvious crack was presented in S-NMC811 cathode without Cl doping (Figure 3d).

## 3. Conclusion

The major challenge of $Li_6PS_5Cl$ sulfide electrolyte is the instability to both Li anode and NMC811 cathode. We enhanced Li dendrite suppression capability of $Li_6PS_5Cl$ by mixing small amount (0.32 wt%) of electronic insulative $CuF_2$-$LiNO_3$, which in-situ forms mixed conductive lithiophobic LiF-$Li_3N$-Cu interface layer at $Li_6PS_5Cl$/Li interface. This interlayer enables the CCD to increase from 0.4 mA $cm^{-2}$/0.4 mAh $cm^{-2}$ for Li|$Li_6PS_5Cl$|Li cell to 1.4 mA $cm^{-2}$/1.4 mAh $cm^{-2}$ for Li|$Li_6PS_5Cl$-$CuF_2$-$LiNO_3$|Li cell at room temperature. In the single-crystalline NMC811 (S-NMC811) cathode, small amount of $AlF_3$ was mixed in $Li_6PS_5Cl$-$CuF_2$-$LiNO_3$ electrolyte and $Cl^-$ was doped on the S-NMC811 surface to suppress the side reaction between S-NMC811 and $Li_6PS_5Cl$-$CuF_2$-$LiNO_3$-$AlF_3$. All-solid-state Cl@S-NMC811-$Li_6PS_5Cl$-$CuF_2$-$LiNO_3$-$AlF_3$|$Li_6PS_5Cl$-$CuF_2$-$LiNO_3$|Li cell achieved a high capacity retention of 69.4% after 100 cycles at 2.55 mA $cm^{-2}$/2.55 mAh $cm^{-2}$.

## Supporting Information

Supporting Information is available from the Wiley Online Library or from the author.

## Acknowledgements

This work was supported by Department of Energy (DOE) under Award number DEEE0008856. H.W. also acknowledges support of ARPA-E under Award of DE-AR0000781.

## Conflict of Interest

The authors declare no conflict of interest.

## Data Availability Statement

The data that support the findings of this study are available from the corresponding author upon reasonable request.

## Keywords

all-solid-state lithium battery, cathode/electrolyte interphase, halogen doping, single-crystalline $LiNi_{0.8}Co_{0.1}Mn_{0.1}O_2$, solid-electrolyte interphase

Received: October 26, 2021
Revised: December 7, 2021
Published online:

[1] Y. Bi, J. Tao, Y. Wu, L. Li, Y. Xu, E. Hu, B. Wu, J. Hu, C. Wang, J.-G. Zhang, Y. Qi, J. Xiao, *Science* **2020**, *370*, 1313.
[2] X. Li, Z. Ren, M. Norouzi Banis, S. Deng, Y. Zhao, Q. Sun, C. Wang, X. Yang, W. Li, J. Liang, X. Li, Y. Sun, K. Adair, R. Li, Y. Hu, T.-K. Sham, H. Huang, L. Zhang, S. Lu, J. Luo, X. Sun, *ACS Energy Lett.* **2019**, *4*, 2480.
[3] H.-H. Ryu, B. Namkoong, J.-H. Kim, I. Belharouak, C. S. Yoon, Y.-K. Sun, *ACS Energy Lett.* **2021**, *6*, 2726.
[4] X. Li, W. Peng, R. Tian, D. Song, Z. Wang, H. Zhang, L. Zhu, L. Zhang, *Electrochim. Acta* **2020**, *363*, 137185.
[5] X. Liu, B. Zheng, J. Zhao, W. Zhao, Z. Liang, Y. Su, C. Xie, K. Zhou, Y. Xiang, J. Zhu, H. Wang, G. Zhong, Z. Gong, J. Huang, Y. Yang, *Adv. Energy Mater.* **2021**, *11*, 2003583.
[6] C. Wang, K. R. Adair, J. Liang, X. Li, Y. Sun, X. Li, J. Wang, Q. Sun, F. Zhao, X. Lin, R. Li, H. Huang, L. Zhang, R. Yang, S. Lu, X. Sun, *Adv. Funct. Mater.* **2019**, *29*, 1900392.
[7] P. Wang, W. Qu, W. L. Song, H. Chen, R. Chen, D. Fang, *Adv. Funct. Mater.* **2019**, *29*, 1900950.
[8] F. Walther, R. Koerver, T. Fuchs, S. Ohno, J. Sann, M. Rohnke, W. G. Zeier, J. Janek, *Chem. Mater.* **2019**, *31*, 3745.
[9] C. Li, W. H. Kan, H. Xie, Y. Jiang, Z. Zhao, C. Zhu, Y. Xia, J. Zhang, K. Xu, D. Mu, F. Wu, *Adv. Sci.* **2019**, *6*, 1801406.
[10] U.-H. Kim, G.-T. Park, P. Conlin, N. Ashburn, K. Cho, Y.-S. Yu, D. A. Shapiro, F. Maglia, S.-J. Kim, P. Lamp, C. S. Yoon, Y.-K. Sun, *Energy Environ. Sci.* **2021**, *14*, 1573.
[11] Q.-Q. Qiu, S.-S. Yuan, J. Bao, Q.-C. Wang, X.-Y. Yue, X.-L. Li, X.-J. Wu, Y.-N. Zhou, *J. Energy Chem.* **2021**, *61*, 574.
[12] F. Zhao, Q. Sun, C. Yu, S. Zhang, K. Adair, S. Wang, Y. Liu, Y. Zhao, J. Liang, C. Wang, X. Li, X. Li, W. Xia, R. Li, H. Huang, L. Zhang, S. Zhao, S. Lu, X. Sun, *ACS Energy Lett.* **2020**, *5*, 1035.
[13] J. Kasemchainan, S. Zekoll, D. S. Jolly, Z. Ning, G. O. Hartley, J. Marrow, P. G. Bruce, *Nat. Mater.* **2019**, *18*, 1105.
[14] F. Han, A. S. Westover, J. Yue, F. Wang, M. Chi, D. N. Leonard, N. J. Dudney, H. Wang, C. Wang, *Nat. Energy* **2019**, *4*, 187.
[15] X. Ji, S. Hou, P. Wang, X. He, N. Piao, J. Chen, X. Fan, C. Wang, *Adv. Mater.* **2020**, *32*, 2002741.
[16] X. Fan, X. Ji, F. Han, J. Yue, J. Chen, L. Chen, T. Deng, J. Jiang, C. Wang, *Sci. Adv.* **2018**, *4*, eaau9245.
[17] R. Xu, F. Han, X. Ji, X. Fan, J. Tu, C. Wang, *Nano Energy* **2018**, *53*, 958.
[18] C. Yang, H. Xie, W. Ping, K. Fu, B. Liu, J. Rao, J. Dai, C. Wang, G. Pastel, L. Hu, *Adv. Mater.* **2019**, *31*, 1804815.
[19] H. Duan, W. P. Chen, M. Fan, W. P. Wang, L. Yu, S. J. Tan, X. Chen, Q. Zhang, S. Xin, L. J. Wan, Y. G. Guo, *Angew. Chem., Int. Ed.* **2020**, *132*, 12167.
[20] Y. Zhong, Y. Xie, S. Hwang, Q. Wang, J. J. Cha, D. Su, H. Wang, *Angew. Chem., Int. Ed.* **2020**, *59*, 14003.
[21] Y. Lu, C. Z. Zhao, H. Yuan, X. B. Cheng, J. Q. Huang, Q. Zhang, *Adv. Funct. Mater.* **2021**, *31*, 2009925.
[22] A. Shapira, O. Tiurin, N. Solomatin, M. Auinat, A. Meitav, Y. Ein-Eli, *ACS Appl. Energy Mater.* **2018**, *1*, 6809.
[23] S.-H. Lee, C. S. Yoon, K. Amine, Y.-K. Sun, *J. Power Sources* **2013**, *234*, 201.
[24] J. Zheng, M. Gu, J. Xiao, B. J. Polzin, P. Yan, X. Chen, C. Wang, J.-G. Zhang, *Chem. Mater.* **2014**, *26*, 6320.
[25] L. Chen, Y. Yang, Z. Wang, Z. Lin, J. Zhang, Q. Su, Y. Chen, W. Chen, Y. Lin, Z. Huang, *J. Alloys Compd.* **2017**, *711*, 462.
[26] Y. Li, Q. Zhang, T. Xu, D. Wang, D. Pan, H. Zhao, Y. Bai, *Ceram. Int.* **2018**, *44*, 4058.